Geochemistry Geophysics Geosystems G3
AN ELECTRONIC JOURNAL OF THE EARTH SCIENCES
Published by AGU and the Geochemical Society

Article
Volume 8, Number 2
6 February 2007
Q02001, doi:10.1029/2006GC001427
ISSN: 1525-2027

Experimental evaluation of in situ CO_2-water-rock reactions during CO_2 injection in basaltic rocks: Implications for geological CO_2 sequestration

Juerg M. Matter and Taro Takahashi
Geochemistry, Lamont-Doherty Earth Observatory of Columbia University, 61 Route 9W, Palisades, New York 10964, USA (jmatter@ldeo.columbia.edu; taka@ldeo.columbia.edu)

David Goldberg
Borehole Research, Lamont-Doherty Earth Observatory of Columbia University, 61 Route 9W, Palisades, New York 10964, USA (goldberg@ldeo.columbia.edu)

[1] Deep aquifers are potential long-term storage sites for anthropogenic CO_2 emissions. The retention time and environmental safety of the injected CO_2 depend on geologic and physical factors and on the chemical reactions between the CO_2, the aquifer water, and the host rocks. The pH buffer capacity of the aquifer water and the acid neutralization potential of the host rocks are important factors for the permanent stabilization of the injected CO_2. Mafic rocks, such as basalt, which primarily consists of Ca, Mg silicate minerals, have a high acid neutralization capacity by providing alkaline earth elements that form stable carbonate minerals. The carbonate minerals formed thus sequester CO_2 in a chemically stable and environmentally benign form. In this study, we present results from a small-scale CO_2 injection test in mafic and metasedimentary rocks. The injection test was conducted using a single-well push-pull test strategy. CO_2 saturated water (pH = 3.5) was injected into a hydraulically isolated and permeable aquifer interval to study the acid neutralization capacity of Ca, Mg silicate rocks and to estimate in situ cation release rates. Release rates for Ca, Mg, and Na were calculated by use of solute compositions of water samples retrieved after the CO_2 injection, the incubation time of the injected solution within the aquifer, and geometric estimates of the reactive surface area of the host rocks. Our results confirm rapid acid neutralization rates and water-rock reactions sufficient for safe and permanent storage of CO_2. Carbonic acid was neutralized within hours of injection into a permeable mafic aquifer by two processes: mixing between the injected solution and the aquifer water, and water-rock reactions. Calculated cation release rates decrease with increasing pH that is confirmed by laboratory-based experiments. Large differences between release rates obtained from the field and laboratory experiments may be mainly due to uncertainties in the estimation of the reactive surface area in the field experiment and in hydrological and geological factors. Our results underscore the importance of defining bulk rock dissolution rates under in situ conditions in order to evaluate target formations for permanent mineral sequestration of carbon dioxide.

Components: 11,006 words, 8 figures, 7 tables.

Keywords: carbon dioxide sequestration; rock-water reactions; low temperature geochemistry.

Index Terms: 1009 Geochemistry: Geochemical modeling (3610, 8410); 1012 Geochemistry: Reactions and phase equilibria (3612, 8412); 1899 Hydrology: General or miscellaneous.

Received 21 July 2006; **Revised** 21 October 2006; **Accepted** 9 November 2006; **Published** 6 February 2007.

Matter, J. M., T. Takahashi, and D. Goldberg (2007), Experimental evaluation of in situ CO_2-water-rock reactions during CO_2 injection in basaltic rocks: Implications for geological CO_2 sequestration, *Geochem. Geophys. Geosyst.*, *8*, Q02001, doi:10.1029/2006GC001427.

1. Introduction

[2] The reduction of industrial CO_2 emissions and the stabilization of the atmospheric CO_2 concentration are considered to be one of the main challenges of this century [e.g., *Hoffert et al.*, 2002; *Lackner*, 2003; *Pacala and Socolow*, 2004]. This may be accomplished by conservation and improved efficiency of energy generating systems, as well as by the recovery of industrial CO_2 and its sequestration in geological formations and oceans [*Intergovernmental Panel on Climate Change* (*IPCC*), 2005]. Among currently proposed storage techniques, injection into deep geological formations, in particular saline aquifers, is one of the most promising alternatives [e.g., *Bachu et al.*, 1994; *Bergman and Winter*, 1995; *Hitchon*, 1996; *Holloway*, 2001; *IPCC*, 2005]. Deep aquifers are important due to their large potential storage capacity and geographic ubiquity. The success of this option will be measured by the storage duration and the risk for leakage [e.g., *Hawkins*, 2004; *Rochelle et al.*, 2004]. Carbon dioxide is injected into deep geologic formations typically as a supercritical fluid in addition to the water phase already present. The fate of the injected CO_2 within the aquifer once injected will be governed by its interaction with the aquifer water and the aquifer host rocks. According to *Gunter et al.* [2004], storage occurs via two main trapping mechanisms: (1) physical trapping and (2) geochemical trapping. The first mechanism includes the storage of CO_2 beneath impermeable cap rocks or stratigraphic traps associated with unconformities and salt domes. Additional types of physical or hydrogeological trapping is provided by the slow flow rates and long residence times of brines within deep aquifers and the gradual dissolution of CO_2 into these brines as well as by capillary trapping of the injected CO_2 in the pore space [*IPCC*, 2005]. The injected CO_2 may therefore be physically trapped over geological timescales [*Bachu et al.*, 1994].

[3] Dissolution of CO_2 into the brine and subsequent formation of carbonic acid leads to the second mechanism which involves chemical reactions of carbonic acid with the host rock and the formation of new stable carbonate minerals. This mechanism, however, requires host rocks with a high acid neutralization potential [*Baines and Worden*, 2004]. Rocks rich in calcium and magnesium silicate minerals can neutralize acids by providing such cations as Ca^{2+}, Mg^{2+}, Fe^{2+} that may form stable carbonate phases in the presence of CO_2 [*Gunter and Perkins*, 1993]. Most typical injection sites with sedimentary host rocks have mineralogy that is dominated by quartz and aluminosilicate minerals poor in alkaline earth elements and results in a low mineral carbonation potential. Limestones neutralize acids effectively, but release CO_2 in the process. Hence their effectiveness for CO_2 sequestration is limited. In contrast, mafic rocks, such as basalt are rich in magnesium and calcium silicate minerals providing high potential of geochemical trapping by mineral carbonation.

[4] A general geochemical trapping model in basalt hosted aquifers is illustrated in equations (1) to (3) [after *Takahashi et al.*, 2000]. Deep groundwater in basaltic rock is rich in Na^+, Ca^{2+}, Mg^{2+} ions [*Spane and Webber*, 1995; *McLing et al.*, 2001]. When CO_2 is injected into such waters, these ions react with CO_2 to precipitate carbonate minerals according to reaction (1):

$$\left(Ca^{2+}, Mg^{2+}\right) + CO_2 + H_2O = (Ca, Mg)CO_3 + 2H^+ \quad (1)$$

Per mol of carbonate mineral precipitated, 2 moles of H^+ ions are produced and reaction (1) will not proceed to the right unless the H^+ ions are neutralized. One way of neutralizing the H^+ ions is by reaction with the host rock. This reaction may be expressed by equations (2) and (3) with the assumptions that the chemical composition of basalt is approximated by olivine and Ca-plagioclase.

$$Mg_2SiO_4(s) + 4H^+ = 2Mg^{2+} + 2H_2O + SiO_2 \quad (2)$$

$$CaAl_2Si_2O_8 + 2H^+ + H_2O = Ca^{2+} + Al_2Si_2O_5(OH)_4 \quad (3)$$

Since the rate of carbonate mineral precipitation (1) is known to be fast, the extent of solid carbonate formation depends primarily on the rate of reaction of (2) to (3), i.e., the dissolution rate of Ca, Mg-silicate minerals.

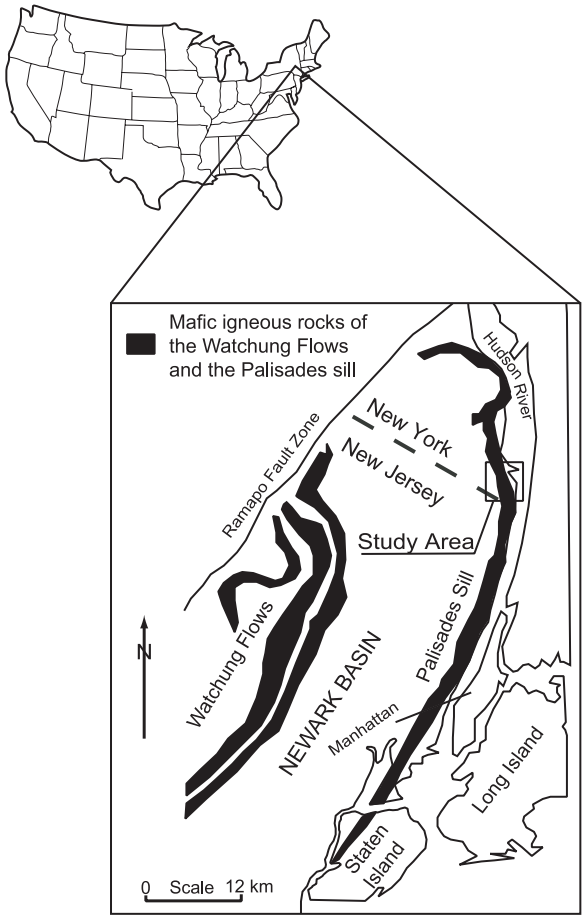

Figure 1. Schematic geological map of the Newark Basin, showing the mafic extrusive rocks of the Watchung flows, the intrusives of the Palisades Sill, and the location of the study area.

[5] With the exception of a few laboratory studies [*Pearce et al.*, 1996; *Gunter et al.*, 1997; *Sass et al.*, 2001; *McGrail et al.*, 2003; *Kaszuba et al.*, 2005] most of the previous experimental dissolution studies on mineral-water-CO_2 reactions have been performed on either monomineralic samples and/or with high fluid-rock ratios [e.g., *Giammar et al.*, 2005; *Carroll and Knauss*, 2005]. It is well known, however, that weathering rates of silicate minerals defined in the laboratory differ from field-derived rates by as much as several orders of magnitude [*Velbel*, 1993; *White and Brantley*, 2003].

[6] In this study, we investigate the extent of in situ water-rock reactions in basaltic rocks after injection of CO_2 in a natural environment to understand dissolution rates of Ca, Mg silicate bearing rocks. Since the dissolution rate of Ca, Mg silicates is one of the main limiting steps in mineral trapping of CO_2, the primary objectives of this study are the characterization of the water-rock reactions and the subsequent estimation of in situ bulk rock dissolution rates, i.e., Ca, Mg release rates, in a natural environment.

[7] Important implications for CO_2 sequestration in basalt-hosted aquifers are discussed in light of the observed geochemical reactions and dissolution rates. We performed a small-scale CO_2 injection experiment using a single-well push-pull test strategy in dolerite rocks in the Palisades Sill and the underlying Newark Basin sedimentary rocks. We will discuss results from the first injection test conducted during summer 2004.

2. Single-Well "Push-Pull" Tests

[8] Since 2004 several single-well push-pull tests were conducted in the contact zone between the Palisades Sill and the underlying Newark Basin sediments at the Lamont-Doherty Earth Observatory test well site in the NE part of the Newark rift basin (Figure 1). Prior to the injection tests, extensive subsurface characterization work has been performed. Borehole geophysical and hydrogeological methods were used to define the subsurface and detect suitable injection intervals [*Goldberg and Burgdorff*, 2005; *Matter et al.*, 2005]. At the test site, the Palisades Sill exhibits a thickness of 230 meters and consists of dolerite rich in Ca-plagioclase and pyroxenes (diopside, hypersthene). The tests were conducted in the olivine-free part of the sill. The whole rock chemistry and the observed mineralogy based on thin section analysis of the dolerite are summarized in Table 1. The contact zone between the dolerite and the underlying sediments with a thickness of approximately 10 to 20

Table 1. Chemical Composition and Normative Mineralogy of the Palisades Sill Dolerite

	Rock Chemistry Dolerite, wt%	Observed Mineralogy[a]
SiO_2	52.2	quartz
Al_2O_3	14.65	plagioclase
CaO	10.43	alkalifeldspar
MgO	7.91	hypersthene
Na_2O	2.14	diopside
K_2O	0.69	magnetite
Fe_2O_3	10.14	ilmenite
MnO	0.15	
TiO_2	1.28	
P_2O_5	0.17	
Cr_2O_3	0.07	
LOI[b]	0.2	

[a] Based on thin section analysis.
[b] LOI, loss on ignition.

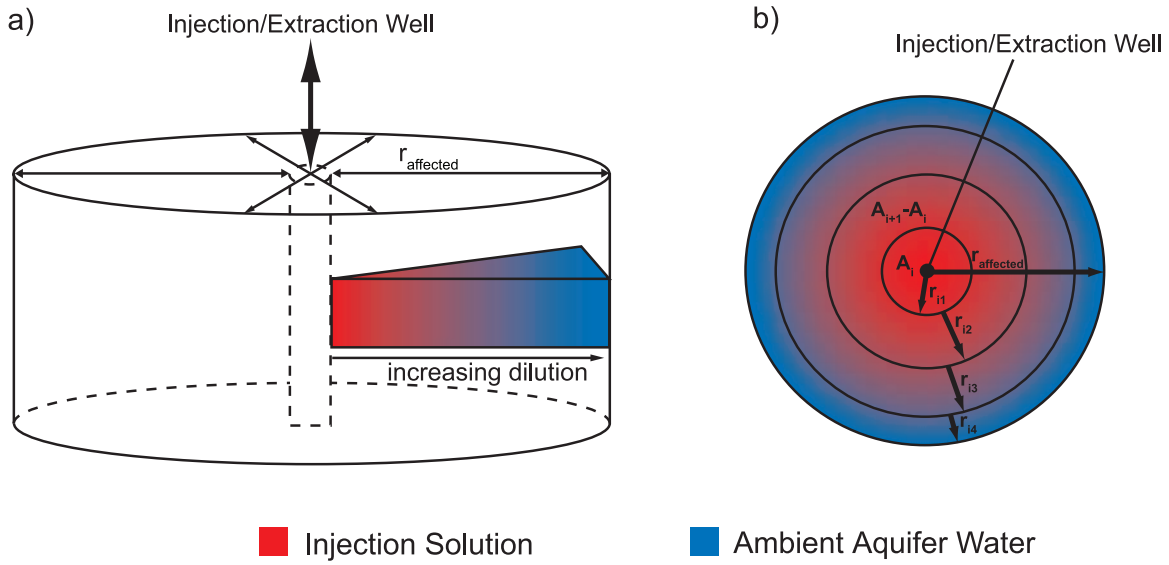

Figure 2. Single-well push-pull test schematic indicating (a) the proportion of aquifer close to the injection/extraction well with increasing dilution away from the well and (b) the plan view of the radially symmetrical aquifer model (modified with permission from *Istok et al.* [2002]).

meters is characterized by the occurrence of chilled dolerite and contact-metamorphosed sedimentary rocks (hornfels). Below the contact zone, alternating layers of sandstone, siltstone and mudstones of the Triassic Newark Series are the dominant rocks. The permeability of the dolerite as well as the sedimentary rocks is defined by secondary porosity (fractures), whereas only two distinct zones of increased hydraulic conductivity, which correlate with the contact zone and the chilled dolerite, were detected [*Matter et al.*, 2005]. With the exception of these two zones of increased permeability, the dolerite and the underlying sedimentary rocks have low permeability.

[9] The CO_2 injection tests were performed as single-well push-pull tests of a similar type described by *Istok et al.* [1997]. Single-well push-pull tests have been used to quantitatively determine a wide range of aquifer physical, chemical and biological processes [e.g., *Istok et al.*, 1997; *Burbery et al.*, 2004]. The test consists of two stages: a "push" stage, where a well-mixed fluid is injected rapidly into the saturated zone of the aquifer through a single well. In this study, a target injection zone (dolerite-sediment contact zone) of 8-meter thickness was hydraulically isolated with straddle packers placed above and below the zone, and 1400 liters (1.4 m^3) of fluid was injected over a period of 3 hours. The temperature of the ambient groundwater within the injection interval was 15°C. Pressure transducers above, within and below the interval monitored the injection as well as the evolution of the hydraulic heads within these intervals during and after the injection. The injection solution was prepared in a polyethylene tank at the wellhead using local tap water, spiked with salt tracers (328 mg/L NaCl, 10 mg/L KBr). The solution was then continuously pumped into the injection apparatus consisting of two stainless steel pressure vessels with a build-in piston pump for injection. It was equilibrated with CO_2 ($P_{CO2} \sim$ 8 atm) in the pressure vessels. After the injection of the spiked solution, 208 liters of unspiked tap water (chaser solution) was injected to flush the solute from the wellbore into the formation. We assumed that the injection solution flowed radially outward from the well into the hydraulically isolated zone of the aquifer and it mixed with the aquifer water as it was injected (Figure 2). Within the aquifer, the injected solution was mixed with the surrounding aquifer water in increasing proportions as it was pushed away from the well. Water samples from the ambient aquifer water within the isolated interval and from the injection and chaser solution were taken before and after injection for chemical analysis. After a 7-day incubation period during which the injection solution/aquifer water mixture was allowed to drift with the natural groundwater flow, the "pull" phase was initiated by pumping water out of the well. The injection solution/aquifer water mixture flowed radially inward toward the well (Figure 2). We pumped the water at a rate of 12 L/min until the tracer concen-

trations were close to pre-test background levels. At the wellhead, the extracted injection solution/aquifer water mixture passed through a flow-through cell in which electrical conductivity, temperature and pH were continuously monitored. Water samples were collected at incremental time intervals from the discharge stream at the wellhead for tracer and solute analysis. The elapsed time and the volume extracted were recorded automatically by computer, and the "pull" phase was completed after about 20 hours.

3. Analytical Methods

[10] A total of 30 water samples were collected in polyethylene vials for ion analyses. All samples were filtered with 0.2 μm nylon filters. Minor and major cation concentrations were measured by ICP-AES at the XRAL laboratory in Toronto, Canada. Multiplicate sample analysis revealed an average reproducibility of ±0.04 mmol/L. Anions were analyzed by ion chromatography (Dionex DX-100) using an IonPac AS14A column with a carbonate/bicarbonate eluent. The analytical precision was ±0.08 mmol/L. In addition to the ion analysis, separate samples were collected in evacuated glass flasks (~250 ml), equipped with a stopcock at each end of the flask for the determination of the total dissolved CO_2. The mass of sampled water was determined by weighing before and after analysis in the laboratory. In the field, the flasks were connected to the sampling line (i.e., small diameter hose) which was, in turn, connected to the submersible pump within the packed-off interval. The glass flasks were filled with groundwater up to 1 atm pressure, leaving a head space of approximately 25% of the bottle volume. In the laboratory, CO_2 within the groundwater was analyzed using a Lamont coulometer [*Chipman et al.*, 1993]. The mass of CO_2 within the head space was estimated. The total dissolved CO_2 concentration was then calculated as the sum of the dissolved CO_2 within the water and the CO_2 within the head space.

4. Data Analysis

[11] Measured solute concentrations enabled breakthrough curves for each solute to be plotted. The background solute concentrations were subtracted from the measured values to account for pre-injection concentrations in the ambient aquifer water. All solute concentrations in the breakthrough curves are plotted as dilution ratios, which are defined as $(C_{measured} - C_{background})/(C_{injected})$. The chloride breakthrough curve is used to calculate recovery percentage for the injected solution (extracted mass/injected mass x 100%) and as a reference point for hydraulic factors such as solute losses due to advection, dispersion and diffusion. Breakthrough curves of reactive solutes (Ca, Mg, Na) are used to quantify bulk rock dissolution. The total mass of all recovered solutes was derived by integration of the breakthrough curves, and the total mass of solutes obtained by water-rock reactions was derived from mass balance calculations using the dilution factors calculated from chloride concentrations. The rate of acid neutralization is reflected in the rate of change in the corrected solute concentrations. Thus average bulk rock dissolution rates or cation release rates were calculated using the following rate equation:

$$R = C_{react}(t) \cdot V_{pumped}(t)/t_r \cdot A \quad (4)$$

where R is the release rate (mmol/cm^2/hour), C_{react} is the dilution corrected concentration of the specific solute at time t (mmol/L), $V_{pumped}(t)$ is the volume of injection solution/aquifer water mixture pumped at time t, A is the reactive surface area (cm^2), and t_r is the incubation time (hour). C_{react} is defined as the measured concentration (C_{meas}) at time t minus the concentration based on mixing (C_{mix}) at time t. The incubation time is defined as the elapsed time between the injection stopped and the sample collection time. The reactive surface area was derived from geometrical estimates of the physical surface area, which are based on borehole televiewer data on fracture density and geometry (see chapter below). Fracture density is assumed to be uniform over the test interval and the aquifer rock in the test interval is considered as a homogenous, isotropic confined aquifer with constant thickness [*Matter et al.*, 2005]. The aquifer volume influenced by the push-pull process is estimated assuming (1) a radially symmetrical flow field around the injection well (cylindrical model) and (2) an effective porosity of 5%, which is based on borehole geophysical measurements (Figure 2). Since the first parcel of injected solution travels a greater radial distance from the injection point than the last one, each extracted water sample is representative for a specific region of influence (i.e., aquifer volume) with a specific radial distance (r_i) from the well. The aquifer volume and radial distance for the each cylinder was computed assuming the radially symmetrical model. The reactive surface area (A_i) of each specific cylindrical aquifer volume was

Table 2. Water Chemistry From Single-Well Push-Pull Experiment[a]

Sample	Time Since Injection Stopped, hours	Total Pumped Volume, liters	pH[b]	Na, mmol/L	Mg, mmol/L	K, mmol/L	Ca, mmol/L	SiO_2, mmol/L	Sr, mmol/L	Cl, mmol/L	SO_4, mmol/L	NO_3, mmol/L	TCO_2, mmol/L
071404_1	162.17	82.8	6.31	2.64	0.52	0.08	2.32	0.43	0.0042	3.78	0.28	0.010	–
071404_2	162.42	378.6	5.90	6.39	0.57	0.09	6.71	0.40	0.0083	3.96	0.32	0.061	50.80
071404_3	163.25	674.3	5.94	6.93	0.48	0.09	5.87	0.40	0.0084	3.53	0.31	0.045	44.20
071404_4	164.67	1088.4	5.99	6.73	0.42	0.08	5.00	0.38	0.0077	3.29	0.36	0.038	38.10
071404_5	166.67	1561.6	6.07	6.76	0.35	0.07	4.24	0.37	0.0070	3.31	0.47	0.028	31.70
071404_6	169.42	2034.8	6.13	6.29	0.28	0.07	3.45	0.36	0.0060	2.81	0.42	0.014	23.80
071404_7	172.83	2507.9	6.19	5.99	0.24	0.06	2.92	0.34	0.0052	2.68	0.47	0.015	
071404_8	176.92	2981.2	6.27	5.90	0.21	0.06	2.57	0.34	0.0047	2.44	0.58	0.011	15.60
071404_9	182.00	3690.9	6.38	5.43	0.16	0.05	1.99	0.32	0.0037	2.12	0.38	0.007	–
071404_10	187.83	4223.3	6.45	5.19	0.13	0.05	1.71	0.31	0.0032	2.23	0.46	0.007	9.69
071404_11	195.17	5288.0	6.56	4.91	0.10	0.04	1.43	0.30	0.0026	1.81	0.42	0.005	7.74
071504_1	204.00	5641.5	6.48	4.86	0.13	0.05	1.99	0.31	0.0032	1.98	0.45	0.006	–
071504_2	212.83	5824.5	6.72	4.62	0.08	0.04	1.16	0.30	0.0020	1.91	0.44	0.003	5.20
071504_3	226.67	10431.8	6.92	4.23	0.05	0.03	0.71	0.28	0.0012	1.79	0.47	na	4.90
071504_4	242.00	16333.8	7.01	4.08	0.04	0.03	0.62	0.28	0.0011	1.73	0.47	na	–
071604_1	244.50	18194.9	7.07	4.12	0.04	0.03	0.65	0.28	0.0011	1.84	0.55	na	–
071604_2	248.50	23027.3	7.32	3.93	0.03	0.03	0.42	0.27	0.0007	1.95	0.50	na	2.30
071904_1	254.75	27014.9	7.09	3.54	0.07	0.05	0.74	0.39	0.0013	2.25	0.40	na	–
072004_1	275.75	29244.1	8.25	3.66	0.04	0.04	0.38	0.35	0.0009	2.23	0.56	na	1.20
Background	0.00	0	8.41	4.04	0.04	0.03	0.56	0.28	0.0010	1.79	0.45	na	1.20
Injection	0.00	0	3.40	6.77	0.63	0.14	1.94	0.27	0.0040	8.60	0.29	na	325.2[c]

[a] Water chemistry is in mmol/L.
[b] The pH reported is measured at standard temperature (20°C).
[c] TCO_2 was calculated.

estimated using borehole televiewer data, the radial distance and a correction factor (0.6) to account for the 60% recovery of the injected solution (Table 3). It has to be noted that the detection limit of the borehole televiewer for fracture aperture is approximately 1.5mm in this well [*Goldberg and Burgdorff*, 2005]. Since each water sample is representative of one annulus (Figure 2), the reactive surface area of each annulus is defined as $\Delta A = A_{i+1} - A_i$. Finally, the geochemical code PHREEQC (version 2.11) developed by *Parkhurst and Appelo* [1999] was used to evaluate the solubility of rock forming minerals in the test interval and the saturation state of the aquifer water with respect to these rock forming minerals before and after the injection test.

5. Results

5.1. Breakthrough Curves

[12] Chemical properties of the ambient aquifer water, the injected solution, and of the water samples collected during the extraction phase are summarized in Table 2. Breakthrough curves of the solute fractions (Ca, Mg, Na, K, Si and Cl) are illustrated in Figure 3. A curve fitting method (3rd degree polynomial fit) to the chloride breakthrough

Table 3. Mass Balance and Recovery Proportions for Calcium, Magnesium, Silicon, and Chloride[a]

Quantities	Calcium	Magnesium	Sodium	Silicon	Chloride
Injected mass, mol	2.7	0.6	9.5	0.4	12.0
Extracted mass, mol (not dilution corrected)	15.7	0.7	11	0.8	7.2
Mass added by reaction, mol (corrected for 60% recovery)	21.7	1.2	2.5	0.7	0.0
% recovery	–	–	–	–	60.0

[a] The extracted mass is corrected for background concentration in the ambient aquifer water. Chloride was used as the conservative tracer in the single-well push-pull test. The mass added by reaction was corrected for the 60% recovery.

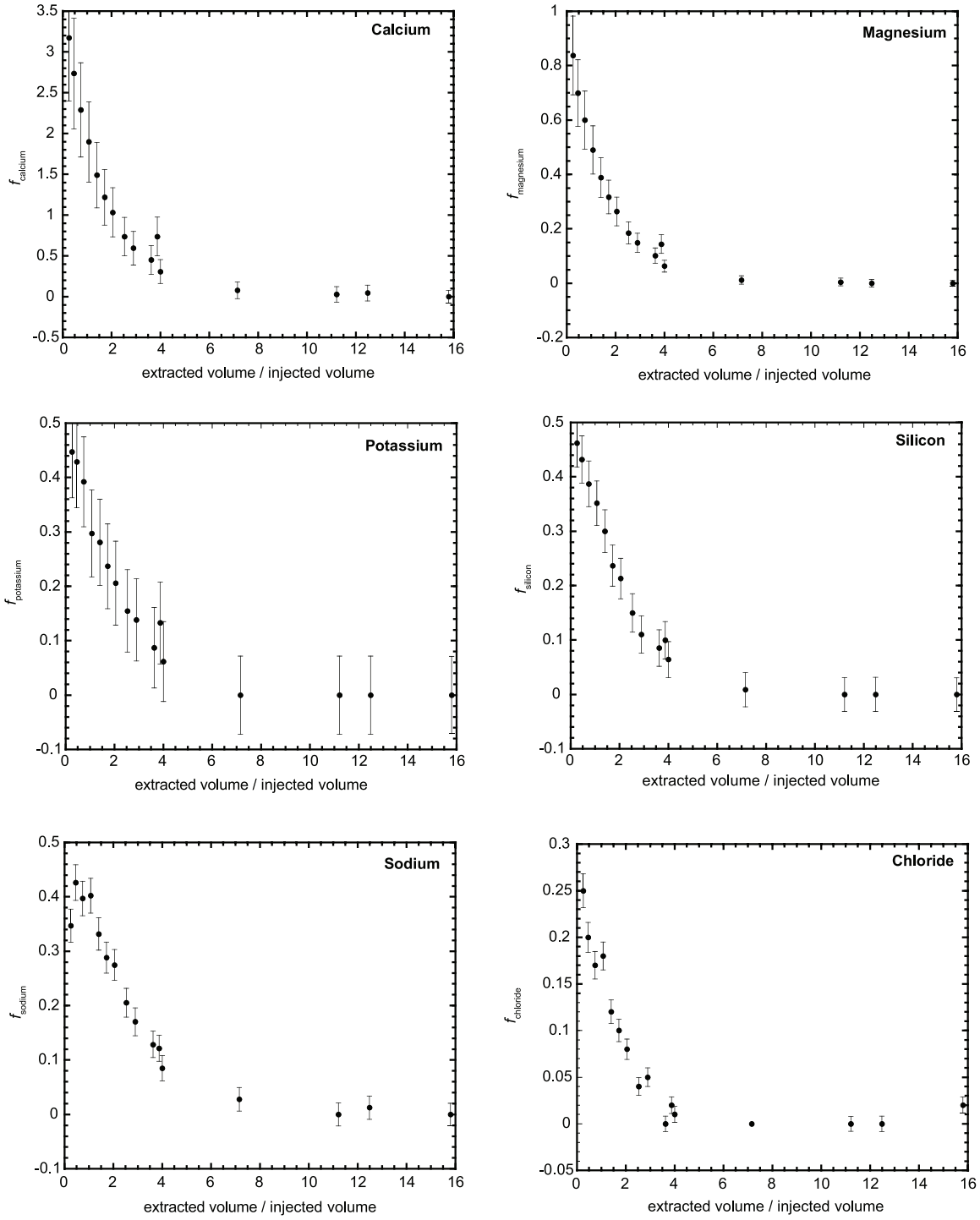

Figure 3. Push-pull test results showing the breakthrough curves of major cations (Ca, Mg, Na, K, Si) and chloride. The measured solute concentrations are reported as a fraction ($f = 1$, 100% injected solution $f = 0$, 100% background water). The propagated error is illustrated for fraction values, whereas the error bar for the extracted volume/injected volume values is smaller than the markers.

curve was used to define when background concentration was reached. Background chloride concentration was reached after the extraction of 5(±0.8)× the injected fluid volume. Similar peak arrival times and shapes of the breakthrough curves suggest similar transport properties of all major solutes during the fluid extraction, "pull" phase. However, the mass of recovered Ca, Mg, Na and Si

Table 4. Computed Carbonate Chemistry of Retrieved Water Samples From the Single-Well Push-Pull Experiment

Sample[a]	TCO_2, mmol/L	pH	T, °C	CO_2(aq), mmol/L	HCO_3^-, mmol/L	CO_3^{2-}, mmol/L	Carbonate Alkalinity,[b] meq/L	Silicate Alkalinity, meq/L	P_{CO2}, atm	Strong Electrol. Charge Balance, meq/L	Unbalanced Charge, meq/L	$SI_{calcite}$
071404_1	–	6.31	14.4	–	–	–	–	–	–	4.05	–	–
071404_2	50.8	5.90	14.3	37.50	12.80	5.63E-04	13.48	2.0E-05	7.90E-01	16.38	2.90	−0.53
071404_3	44.2	5.94	14.4	31.90	11.90	5.66E-04	12.46	3.2E-05	6.80E-01	15.51	3.05	−0.55
071404_4	38.1	5.99	14.5	26.60	11.10	5.84E-04	11.57	3.1E-05	5.60E-01	13.61	2.04	−0.58
071404_5	31.7	6.07	14.7	20.90	10.50	6.56E-04	10.86	3.6E-05	4.50E-01	11.74	0.88	−0.59
071404_6	23.8	6.17	14.8	15.00	8.54	6.00E-04	8.84	3.9E-5	3.20E-01	10.16	1.32	−0.68
071404_7	–	6.20	14.7	–	–	–	–	–	–	–	–	–
071404_8	15.6	6.27	14.9	8.68	6.76	6.38E-04	6.95	5.1E-5	1.90E-01	7.89	0.94	−0.75
071404_9	–	6.38	14.8	–	–	–	–	–	–	–	–	–
071404_10	7.1	6.45	14.7	4.44	5.15	7.07E-04	5.26	6.9E-05	9.55E-02	5.78	0.52	−0.84
071404_11	5.6	6.56	14.8	3.08	4.58	7.98E-04	4.67	8.7E-05	6.61E-02	5.37	0.70	−0.84
071504_1	–	6.47	15.4	–	–	–	–	–	–	–	–	–
071504_2	5.2	6.72	15.0	1.62	3.52	8.91E-04	3.58	1.3E-04	3.55E-02	4.34	0.76	−0.86
071504_3	4.9	6.92	14.8	1.12	3.74	1.45E-03	3.79	1.8E-04	2.40E-02	3.05	−0.74	−0.85
071504_4	–	7.01	14.7	–	–	–	–	–	–	–	–	–
071604_1	–	7.02	14.9	–	–	–	–	–	–	–	–	–
071604_2	2.3	7.32	14.7	0.24	2.04	1.97E-03	2.06	4.5E-04	5.25E-03	1.90	−0.16	−0.91
071904_1	–	7.09	14.8	–	–	–	–	–	–	–	–	–
072004_2	1.2	8.25	14.7	0.02	1.16	9.50E-03	1.22	4.8E-03	3.55E-03	1.20	−0.02	−0.26
Injection	325.2	3.40	14.4	325.00	0.34	4.25E-08	3.37E-04	6.0E-08	7.00	1.20	1.20	0.00
Background	1.2	8.41	14.4	0.01	1.15	0.014	1.22	5.6E-03	2.45E-04	1.20	−0.02	−5.02

[a] Samples are tabulated in order of increasing water recovery (see Table 2).
[b] Includes charged carbonate complexes.

is substantially larger than the recovered mass of Cl, indicating the contribution of ions by dissolution of the aquifer rocks (Table 3). Ferrous ion (Fe^{2+}) concentrations in the retrieved water samples were measured but not used in the overall analysis because concentrations were biased by the downhole equipment (contamination from non-stainless steel components). The recovery proportion based on the conservative chloride tracer was 60% (Table 3). Chloride and bromide were the only conservative tracers used in this injection test. The ambient aquifer water has a background concentration of 1.79 mmol/L of chloride and a bromide concentration below-the-detection limit (5×10^{-4} mmol/L) for the analytical system used. The concentration of chloride and bromide in the injection solution was 8.6 mmol/L and 0.12 mmol/L, respectively. Due to poor reproducibility in bromide measurements, bromide could not be used as a tracer in this experiment. The similarity between the chloride and the cation breakthrough curves, however, allows the measured chloride concentration to adjust the measured major cation concentrations for dilution. Furthermore, the shapes of the breakthrough curves, and especially, the short-time arrival of the peak concentrations are attributed to the hydrodynamics of the push-pull test and the aquifer properties in the test interval. Using the breakthrough volume of 5(±0.8) times of the total injected solution (1.4 m^3), and the radially symmetrical model, the total volume of aquifer rock (with 5% porosity) investigated by the push-pull test was 233(±37) m^3 (= (5 ± 0.8) × 1.4/0.6 × 0.05). The total radial distance ($r_{affected}$) of the 8-meter thick region of influence of the injection/extraction well was ~3.0 m ($\sqrt{233/8\pi}$).

5.2. Carbonate Alkalinity and Total Alkalinity

[13] The total alkalinity (excess cation charges) and carbonate alkalinity (= (HCO_3^-) + 2(CO_3^{2-})), the P_{CO2} as well as the concentration of CO_2(aq), HCO_3^-, and CO_3^{2-} in the retrieved water samples were computed with PHREEQC using the measured ion concentrations, TCO_2, and pH (Table 4). The concentrations of (HCO_3^-) and (CO_3^{2-}) include their complex ions with Ca^{2+}, Mg^{2+}. In addition, saturation indices with respect to calcite are summarized in Table 4. Dissolved CO_2(aq), HCO_3^- and CO_3^{2-} concentrations decrease with increasing retrieved water volume. The computed carbonate

Table 5. Mass Balance Calculations for Calcium, Magnesium, Silicon, and Sodium for Samples 071404_2 to 071404_11

Sample	Reaction Time, hours	Injected Solution Fraction	Native Groundwater Fraction	Ca_{meas}, mmol/L	Ca_{mix}, mmol/L	Ca_{react}, mmol/L	Mg_{meas}, mmol/L	Mg_{mix}, mmol/L	Mg_{react}, mmol/L	Si_{meas}, mmol/L	Si_{mix}, mmol/L	Si_{react}, mmol/L	Na_{meas}, mmol/L	Na_{mix}, mmol/L	Na_{react}, mmol/L
071404_2	162.42	0.32	0.68	6.71	1.00	5.71	0.57	0.23	0.34	0.41	0.28	0.13	6.39	4.91	1.48
071404_3	163.25	0.26	0.74	5.86	0.92	4.94	0.48	0.2	0.28	0.40	0.28	0.12	6.93	6.06	2.18
071404_4	164.67	0.22	0.78	5.00	0.86	4.14	0.42	0.17	0.25	0.38	0.28	0.10	6.73	4.64	2.09
071404_5	166.67	0.22	0.78	4.25	0.86	3.38	0.35	0.17	0.18	0.37	0.28	0.09	6.76	4.64	2.12
071404_6	169.42	0.15	0.85	3.45	0.77	2.68	0.28	0.13	0.15	0.36	0.28	0.08	6.29	4.45	1.84
071404_7	172.83	0.13	0.87	2.92	0.74	2.18	0.24	0.12	0.12	0.34	0.28	0.06	5.99	4.39	1.60
071404_8	176.92	0.10	0.90	2.56	0.70	1.86	0.21	0.10	0.11	0.34	0.28	0.06	5.90	4.31	1.59
071404_9	182.00	0.05	0.95	1.99	0.63	1.36	0.16	0.07	0.09	0.32	0.28	0.04	5.43	4.18	1.25
071404_10	187.83	0.06	0.94	1.71	0.64	1.07	0.13	0.08	0.05	0.31	0.28	0.03	5.19	4.20	0.99
071404_11	195.17	0.01	0.99	1.43	0.56	0.87	0.10	0.04	0.06	0.30	0.28	0.02	4.91	4.05	0.86

alkalinity in the retrieved water samples varies from 13.48 meq/L to 1.22 meq/L, whereas the calculated P_{CO2} values range from 0.8 atm to 3.55×10^{-4} atm, the level similar to the atmospheric P_{CO2} (Table 4). Values for the total alkalinity or the excess cation charges are between 16.8 to 1.20 meq/L. The difference between the total alkalinity and the carbonate alkalinity is the unbalanced charge (meq/L). The alkalinity contributions from other weak acids including silicic acid are negligibly small, and hence the observed charge unbalance suggests experimental errors (Table 4). Alkalinity contributions from phosphate and borate are not accounted for because their concentrations were not determined.

5.3. In Situ Dissolution Rates

[14] The measured cation concentrations in the retrieved water samples reflect mixing between the ambient aquifer water and the injected solution plus the addition of cations by water-rock reactions; assuming a binary mixing between the injected and ambient waters, $C_{mix} = X \cdot C_{inject} + (1 - X) \cdot C_{ambient}$, where X = fraction of the injected solution estimated from chloride concentrations (Table 5). Fraction of the injected solution (or dilution factor) was calculated with chloride because it appears to behave conservatively in this system. A mixing line between the two end-members was computed and is shown for each cation of interest in Figure 4. The difference between the measured solute concentrations (C_{meas}) and the mixing value (C_{mix}) is attributed to the dissolution of the bulk rock and defined as C_{react} in Table 5. Computations, which account for the dilution and hence for the 60% recovery fraction, show that the following total masses are added by reactions: 21.7 mol of calcium, 1.2 mol of magnesium, 2.5 mol of sodium and 0.7 mol of silicon (Table 3).

5.3.1. Mean Bulk Rock Dissolution Rates

[15] Mean bulk rock dissolution rates were calculated using the total mass transfer, the total incubation time of the injected fluid, and the total reactive surface area of the test interval. To determine the reactive surface area, the physical surface area of fractures within the injected interval is needed. The analysis of digital borehole televiewer fracture logs from the injection site provided quantitative geometrical data of fracture location, dip and aperture [*Goldberg and Burgdorff*, 2005; *Matter et al.*, 2005]. For each detected fracture, the surface area was geometrically estimated assuming a plate-like geometry and using fracture

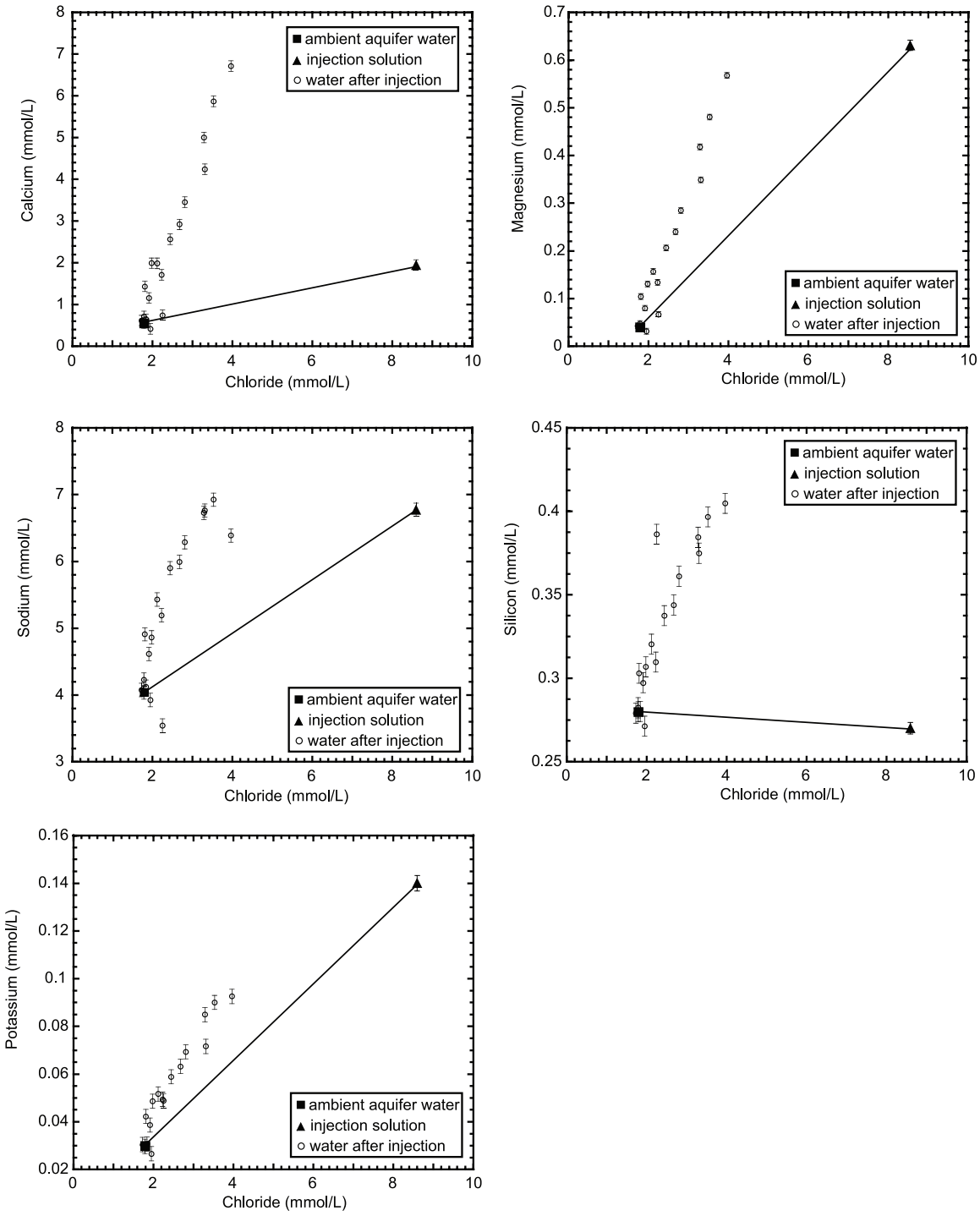

Figure 4. Major cations versus chloride, illustrating the mixing line between the native groundwater and the injected solution as well as the data from water samples extracted after the injection. All extracted water samples are above the mixing line, indicating increased concentration due to dissolution reactions. Error bars indicate the analytical accuracy. Error bars for chloride are smaller than the markers.

aperture and length data from the televiewer log [*Matter et al.*, 2005]. The latter was geometrically calculated using the fracture's dip angle and assumes that the fracture extends a certain radial distance (r_i) away from the injection/extraction well (Figure 5). Hence, using the total radial distance of the region of influence ($r_{affected}$ = 3 m) for each fracture, the calculated total surface area of aquifer

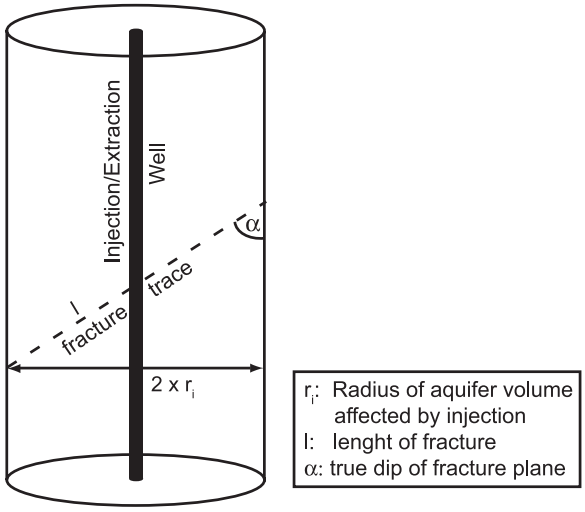

Figure 5. Schematic illustration showing an inclined fracture intersecting the injection/extraction well as well as the cylindrical aquifer volume around the well, which is affected by the push-pull test. The true length of the fracture was geometrically calculated by using the true dip of the fracture plane and the radius of the cylindrical aquifer volume.

rock affected by the push-pull test is 1.35×10^7 cm^2. Mean calcium, magnesium and sodium release rates, calculated using the total masses added by reaction and corrected for the 60% recovery fraction (Table 3), the total surface area and the total incubation time, are 8.93×10^{-6} mmol/cm^2/hour for Ca, 4.95×10^{-7} mmol/cm^2/hour for Mg, and 1.03×10^{-6} mmol/cm^2/hour for Na.

5.3.2. The pH Dependence of Dissolution Rates

[16] Each water sample retrieved through pumping is representative of a specific cylindrical aquifer volume (i.e., annulus). We calculated therefore for each water sample the specific Ca, Mg and Na release rates by using equation (4) and C_{react} (mmol/L), ΔV pumped water (L), incubation time (hour) and specific surface area of each annulus ($\Delta A = A_{i+1} - A_i$), which was corrected for the 60% recovery of the injected solution. The variables to calculate the specific release rates as well as the calculated release rates for each retrieved water samples are summarized in Table 6. The resulting release rates range from 1.73×10^{-5} to 2.23×10^{-6} mmol/cm^2/hour for Ca, and from 1.03×10^{-6} to 1.28×10^{-7} mmol/cm^2/hour for Mg as pH increased from 5.9 to 6.6. Release rates for sodium are between 4.49×10^{-6} to 2.21×10^{-6} mmol/cm^2/hour. The cation release rates decrease

Table 6. Measured and Estimated Input Variables for Equation (4) and Specific Release Rates for Calcium, Magnesium, and Sodium Calculated for Each Retrieved Water Sample[a]

Sample	Pumped Volume, L	Δ Pumped Volume (Annulus), L	Vrock,[b] m^3	Radius (r_i), m	Surface Area, cm^2	Δ Surface Area (Annulus), cm^2	Incubation Time, hours	pH	Ca_{react}, mmol/L	Mg_{react}, mmol/L	Na_{react}, mmol/L	R_{Ca}, mmol/cm^2/h	R_{Mg}, mmol/cm^2/h	R_{Na}, mmol/cm^2/h
071404_2	378.56	378.56	12.62	0.71	764054.43	764054.43	163.42	5.90	5.71	0.34	1.48	1.73E-05	1.03E-06	4.49E-06
071404_3	674.31	295.75	22.48	0.95	1339096.44	575042.01	164.25	5.94	4.94	0.28	0.33	1.55E-05	8.77E-07	1.03E-06
071404_4	1088.36	414.05	36.28	1.20	2177798.81	838702.37	165.67	5.99	4.14	0.25	2.09	1.23E-05	7.45E-07	6.23E-06
071404_5	1561.56	473.20	52.05	1.44	3132106.38	954307.57	167.67	6.07	3.39	0.18	2.12	1.00E-05	5.32E-07	6.27E-06
071404_6	2034.76	473.20	67.83	1.64	4059451.20	927344.82	170.42	6.13	2.68	0.15	1.84	8.02E-06	4.49E-07	5.51E-06
071404_7	2507.96	473.20	83.60	1.82	4996730.47	937279.27	173.83	6.19	2.18	0.12	1.6	6.33E-06	3.49E-07	4.65E-06
071404_8	2981.16	473.20	99.37	1.99	5971248.50	974518.03	177.92	6.27	1.86	0.11	1.59	5.08E-06	3.00E-07	4.34E-06
071404_9	3690.96	709.80	123.03	2.21	7361175.83	1389927.33	183.00	6.38	1.36	0.09	1.25	3.80E-06	2.51E-07	3.49E-06
071404_10	4223.31	532.35	140.78	2.37	8463293.26	1102117.43	188.83	6.45	1.07	0.05	0.99	2.74E-06	1.28E-07	2.53E-06
071404_11	5288.01	1064.70	176.27	2.65	10576922.75	2113629.49	196.17	6.56	0.87	0.05	0.86	2.23E-06	1.28E-07	2.21E-06

[a] Release rates for calcium, magnesium, and sodium are R_{Ca}, R_{Mg}, and R_{Na}, respectively.
[b] Corrected for the 60% recovery of the injected solution.

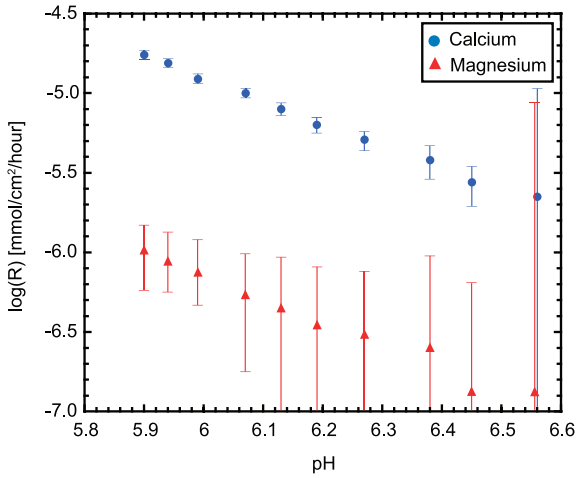

Figure 6. The pH dependence of in situ calcium and magnesium release rates (mmol/cm^2/hour) from the field injection test. The propagated error is illustrated for the release rates, whereas the error bars for the pH values are smaller than the markers. Surface area is considered as a constant, and the error in the surface area estimate is not included in the error propagation calculations.

with increasing pH (Figure 6) and this will be discussed further in the following chapter.

6. Discussion

[17] The ability of basalt and siliciclastic formations to neutralize carbonic acid was demonstrated under in situ conditions with a single-well push-pull test. The injection of a CO_2-saturated solution (P_{CO2} of 8 atm) into a hydraulically isolated interval within the contact zone of the Palisades Sill dolerite and the underlying Newark Basin sediments produced relatively rapid reactions of the host rocks with the injected carbonic acid. As postulated by *Holland et al.* [1986], dissolved carbon dioxide provides protons that accelerate mineral dissolution. Dissolution of the bulk rock material is clearly indicated in this in situ experiment by a shift upward from the mixing lines with dilution of the injected solution by aquifer water. However, the change in ion concentrations decreases with increasing time because of two processes, dilution by mixing and dissolution of bulk rock material, both resulting in decreasing acidity. The effect of mixing of injected fluid with aquifer water was determined by adding a conservative tracer (chloride) and by calculating dilution factors for each water sample. Applying the dilution factors and the measured ion concentrations, mass transfer terms for Ca, Mg, Na and Si were calculated. These indicate that the one of the first water samples (071404_2; Table 5) retrieved after 163 hours post-injection was enriched in Ca 12×, in Mg 14×, in Na 2×, and in silicate 1.5× relative to the pre-injection concentrations.

[18] Using the calculated mass transfer terms of calcium and magnesium, the incubation time, and the calculated surface areas, bulk rock dissolution rates of aquifer material were estimated. It is important to note that only elements, for which no effects of precipitation or sorption reactions occur, may be used to calculate dissolution rates. Therefore saturation index for various mineral species were calculated using the geochemical code PHREEQC (v. 2.11) [*Parkhurst and Appelo*, 1999] and the integrated LLNL thermodynamic database, "thermo.com.V8.R6.230" [*Johnson et al.*, 2000]. The saturation index, SI, was computed by SI = log (IAP/K_T), where IAP is the ion activity product and K_T is the equilibrium constant at temperature T for a specific mineral species. The results reveal that the retrieved water samples are undersaturated with respect to the primary rock forming minerals, calcite and dolomite but are supersaturated with respect to chalcedony (a cryptocrystalline silicate), which can be used as a proxy for silica precipitates in natural groundwater [*Rimstidt*, 1997]. Aluminum in the water samples was not detected (detection limit 10^{-7} mol/L). Assuming an aluminum concentration of 10^{-8} mol/L for the retrieved water samples, the calculated saturation index shows that they are supersaturated with respect to kaolinite, and saturated to slightly supersaturated with respect to Na-, Mg-, or Ca-montmorillonite. We speculate that the aluminum concentration in the groundwater is probably controlled by the formation of clay minerals. In addition, the post-injection silicon concentration may also be affected by clay minerals or silicate precipitation reactions. Therefore silicon release data were not used to estimate bulk rock dissolution rates. Considering the Ca and Mg mass transfer, we assume that the precipitation of clay minerals (montmorillonite) does not significantly affect concentrations, and that the release of these cations reflects the dissolution of the bulk rock.

[19] The in situ experiment demonstrated that cation release rates decrease as pH increases (Figure 6). The pH dependence of dissolution is confirmed by laboratory experiments which were conducted in batch reactors under ambient temperature and pressure conditions (20°C, 1 atm). In the batch experiments, bulk rock samples of dolerite

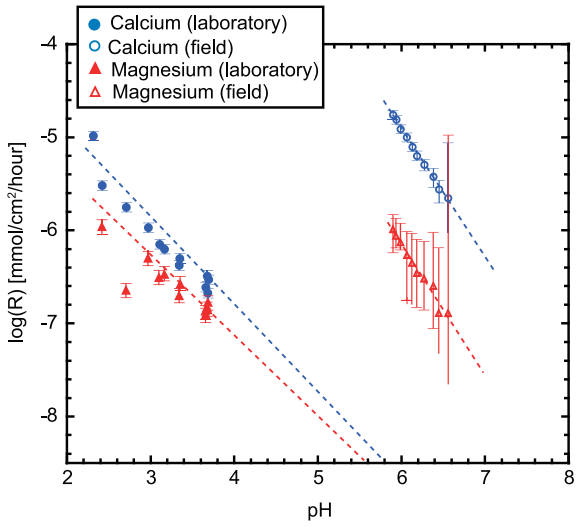

Figure 7. The pH dependence of laboratory and field-based calcium and magnesium release rates (mmol/cm^2/hour). Data plotted represent rates normalized to the geometrical surface area. Dotted lines represent linear regression of all data. Error bars are illustrated for release rate values, whereas error bars for pH values are smaller than the markers.

were crushed and sieved into different size fractions, cleaned ultrasonically, and treated with a weak acid to remove $CaCO_3$. The average size fraction is 0.2 mm and the surface area is geometrically calculated to be 2180 cm^2. The reaction fluid comprises deionized water, Merck grade HCl and NaCl. Through the course of the experiment, the starting pH (pH = 2) was not held constant and was allowed to change as reaction progressed. Cation release rates that are computed using calcium and magnesium concentration measurements, the reaction time, and the computed geometric surface area of the crushed rock grains, range from 1×10^{-5} to 8×10^{-7} mmol/cm^2/hour for calcium and 1×10^{-5} to 1.3×10^{-7} mmol/cm^2/hour for magnesium, with decreasing rates as pH increases to a maximum of pH = 4 (Figure 7).

[20] In Figure 7, dissolution rates are extrapolated linearly beyond this value to pH = 6, to allow a comparison with published dissolution rate data and our field data. Our laboratory derived bulk rock dissolution rate at pH = 6 is about 30 times faster than rates determined for forsterite dissolution at the same pH by *Pokrovsky and Schott* [2000]. The difference may be attributed to differences in the mineralogy and the methods used for surface area determination (B.E.T. versus geometrical estimation). Differences between laboratory and field estimates of dissolution rates, largely due to differing experimental conditions, have been discussed extensively in previous studies [e.g., *Velbel*, 1993; *White and Brantley*, 2003; *Ganor et al.*, 2005]. In Figures 6 and 7, we observe that the field rates are as much as 2.5 orders of magnitude faster for magnesium release and 3.5 orders faster for calcium than the laboratory-based dissolution rates in the same pH range. This is likely the result of several experimental factors, including hydrological and geological aspects. These factors are considered below.

[21] First, unlike the field experiments, which took place in naturally fractured rocks, the reactive surface area in the laboratory experiments consists of fresh exposed surfaces of crushed rock grains. The geometrically estimated surface area of the laboratory samples is more than two orders of magnitude greater than that estimated from in situ natural fractures for the field experiment. Furthermore, the nature of reactive surface in the field experiment is not known. Surface area estimates based on fracture observations in the borehole televiewer data are likely to be underestimates. We assume that the observed physical surface area represents the reactive surface area, although it may be an old fracture coated with clays. Hence this is a highly conservative and probably unrealistic assumption. In addition, the detection limit of the digital borehole televiewer for fracture aperture in this well is approximately 1.5 mm. The contact zone is dominated by fracture porosity greater than this aperture resolution, primarily subhorizontal and subvertical fracturing, which act as the major fluid conduits within the test interval. Hydraulic testing indicates that the contact zone is bounded above and below by low permeability rocks that limit vertical fluid flow out of the contact zone [*Matter et al.*, 2005]. Thus major and minor fractures that could be resolved by the televiewer are included in the surface area estimate, but the small open cracks and tiny fissures less than 1.5 mm wide are not. If these small fractures below the detection limit were present, the reaction surface areas could be as much as one or two orders of magnitude greater than the area estimated. Hence the estimated specific dissolution rate could be reduced by the corresponding magnitude. The reactive surface area estimation remains to be a major source of uncertainty in the specific rate determinations. Roughness of interior fracture surfaces is also not taken into account. Hence the physical surface area estimated using the televiewer data represents a minimum value for the reactive

surface area and implies a maximum in the computed rate constants (see equation (4)). Limited constraints on the in situ surface area therefore translates to uncertainty in the estimated dissolution rates, and may in part explain a large portion of the differences in rates observed in Figures 6 and 7.

[22] Secondly, the field and laboratory experiments agree that Ca is released faster than Mg. However, the difference between the calcium and magnesium release rates are of less than half an order of magnitude for the laboratory experiment, whereas a difference of 1.5 orders of magnitude for the field experiment (Figure 7). The molar concentrations of calcium and magnesium in dolerite are more or less equal (molar Mg/Ca ratio of 1.04), and for the laboratory experiment, the release rates for calcium and magnesium are also roughly equal. In the field experiment, however, release of calcium is strongly preferred over magnesium. Figure 7 shows that the logarithm of dissolution rate observed in the field experiment decreased with increasing pH with a slope of about -1.5 ± 0.25 for Ca, and -1.3 ± 0.3 for Mg. This means that the rate of dissolution increases by about 30 (±15) times with a 10-fold increase in H^+ concentrations for calcium, and 15(±6) times for magnesium. The pH dependence of the dissolution rate for calcium is therefore twice as large as the one for magnesium. Since the molar amounts of calcium and magnesium in the well-crystallized dolerite are equal (Table 1), the two-fold difference in the dissolution rates may be attributed to differences in the sites of these ions in the chilled and glassy dolerite, which was encountered in the field experiment. In contrast, the laboratory experiments with crushed rock grains from well-crystallized dolerite show a log(R) versus pH slope of -0.9 ± 0.1 for both Ca and Mg, indicating that the rate increased by 6 (±2) times with a 10-fold increase in H^+ concentrations. This is in general agreement with previous laboratory studies, which demonstrated that the rate of dissolution decreased by one order of magnitude for an increase in one pH unit [*Pokrovsky and Schott*, 2000; *Hänchen et al.*, 2006].

[23] The similarity of the pH dependence of the rates in the laboratory experiment implies that H^+ has a similar role in the dissolution mechanism for well-crystallized plagioclase and pyroxene group minerals used in the laboratory experiments. Besides the suggested different role of H^+ in the dissolution mechanism of well-crystallized and glassy dolerite, the difference in crystallization between these two types of rocks may introduce a relative preference for ionic release.

[24] Alternatively, additional sources of calcium such as calcium carbonate infill in fractures may add to the total amount of calcium released in the field experiment. A calcium carbonate source for calcium may be detected by stable isotopes analysis ($\delta^{13}C$) on rock and fluid samples [*Assayag et al.*, 2005]. To better constrain the source of calcium, we have recently conducted additional injection tests and $\delta^{13}C$ analysis has been performed on rock and fluid samples. Additional and different mineral sources for calcium and magnesium, an effect of clay mineral precipitation on the release of calcium and magnesium, also cannot be entirely ruled out with the existing data set. To address these observed lab-field differences between calcium and magnesium release rates, complementary laboratory dissolution experiments on rock samples collected from within the injection interval are ongoing. In the previous laboratory experiments hydrochloric acid (HCl) was used to leach the crushed rock samples, whereas in the field experiment carbonic acid (dissolved CO_2) was used. It is therefore questionable to what extent the previous laboratory experiments can be compared with the field experiments. To address this issue, ongoing laboratory experiments will use carbonic acid as a closer complement to the in situ system.

[25] The experimental field data presented in this study address in situ water-rock reactions, with particular emphasis on the calcium and magnesium release after injection of an acidified solution. Since the field experiment took place in a multi-mineral environment consisting of chilled dolerite and recrystallized sedimentary rocks, it is difficult to define quantitatively the sources of magnesium and calcium. We assume that dolerite is the source of Mg ions (pyroxene), whereas the source for Ca ions may be the sedimentary rocks, calcite vein infill in the dolerite, or the dolerite itself. Sample waters have nearly constant and small SO_4^{2-} concentrations, indicating that gypsum is absent. To estimate contributions of these different mineral phases and to interpret net geochemical mass balance reactions, we again utilize the PHREEQC modeling code. Mixing between the injected solution and the ambient aquifer water as well as the mass transfer from water-rock reaction was computed using the water compositions given in Table 2. The mass balance solution uses observed Na, Ca, Mg, Si, and TCO_2 concentrations as constraints and plagioclase (An_{60}), diopside, ensta-

Table 7. Results of the Chemical Mass Transfer Including Mixing and Mineral Dissolution and Precipitation[a]

	Mass Transfer in mmol/kg H_2O				
Sample	Anorthite	Enstatite	Calcite	Quartz	CO_2(g)
071404_2	3.30	0.4	2.54	−0.27	−40.30
071404_3	5.60	0.33	–	−0.21	−33.30
071404_4	4.84	0.29	–	−0.19	−25.73
071404_5	4.34	0.21	–	−0.11	−36.14
071404_6	3.46	0.13	–	–	−28.26
071404_8	2.73	0.1	–	–	−15.3
071404_10	3.85	0.06	−1.9	–	−8.76
071404_11	3.6	0.05	−2.02	–	–

[a] Positive numbers in the mass transfer indicate dissolution of the mineral phase, and negative numbers indicate precipitation.

tite (En_{80}), quartz, kaolinite, and calcite as selected mineral phases as well as CO_2(g). Plagioclase, diopside, enstatite and calcite phases were allowed to dissolve, whereas quartz and kaolinite were added as sinks for silicon and aluminum. The most dominant mineral phases in the system are plagioclase (An_{60}) and pyroxene (En_{80}). Enstatite was defined as the only magnesium source (dolomite and magnesite are not present in the formation) and plagioclase and calcite as the only calcium sources (calcite occurs in veins and fractures, and likely dissolves first). Ca-plagioclase (An_{60}) was also the only sodium source. Elemental analysis of drill cuttings in the test interval reveal $CaCO_3$ values from 0.17 wt% for dolerite, 2.54 wt% for metasedimentary rocks below the injection zone, and 0.44 wt% for the mixed dolerite and metasedimentary rocks within the injection zone. Model solutions matching these mineral mixtures were accepted from the mass balance models when the resulting composition and mineral transfer were consistent with the observed chemical composition and mineral saturation state of the retrieved water samples. For the most abundant mineral phases present (Table 1), the observed composition and mineral saturation states can be reproduced by the mass transfer calculations within an estimated error of 5–10%. Results from the simplest mass balance calculations produced by PHREEQC after the injection of a CO_2-saturated solution indicate that the predicted composition of the retrieved water samples could be due to plagioclase and pyroxene dissolution with minor amounts of calcite dissolution (Table 7). However, *Gislason and Eugster* [1987] demonstrated that basaltic glass dissolves approximately 10× faster than crystalline basalt. We can therefore assume that the most likely source of calcium besides calcite in this study is chilled, glassy dolerite. Mass transfer models for samples 071404_2 to 071404_5, however, require the precipitation of SiO_2, which agrees with estimated saturation index and supersaturation with respect to chalcedony and/or quartz. The measured TCO_2 concentrations cannot be explained without CO_2 loss or precipitation of calcite, although the latter can be ruled out by the undersaturated state for calcite (Table 4). Thus all of the samples with the exception of sample 071404_11 require a CO_2(g) loss to balance the TCO_2 concentration. Since the P_{CO2} of the injected solution (8 atm) and the ambient groundwater (3×10^{-4} atm) within the injected interval differ significantly, mixing of the two may cause a decrease in P_{CO2}. As a result of this analysis, we conclude that some CO_2 was lost during the injection test (Figure 8).

[26] Partial CO_2 loss and the 60% recovery rate of the injected solution, which is based on the chloride tracer may be explained by the existing heterogeneity of the formation and the drift of the injected solution away from the injection point. The injection interval is characterized by a "double porosity," where both pore-scale voids in the matrix rock and meter-scale secondary fracturing of the formation contribute to the total open pore space. The contact zone exhibits higher fracture porosity than the overlying dolerite and underlying sediments. On the basis of this double porosity nature and localized occurrence of fractures in the contact zone, the injection is constrained within this interval and between low transmissivity zones. Flow channeling within the contact zone may occur and result in primary and secondary flow paths (i.e., different flow paths through fracture- and matrix-porosity) during the injection and the recovery phase. Transmissivity contrasts between primary and secondary flow paths could enhance

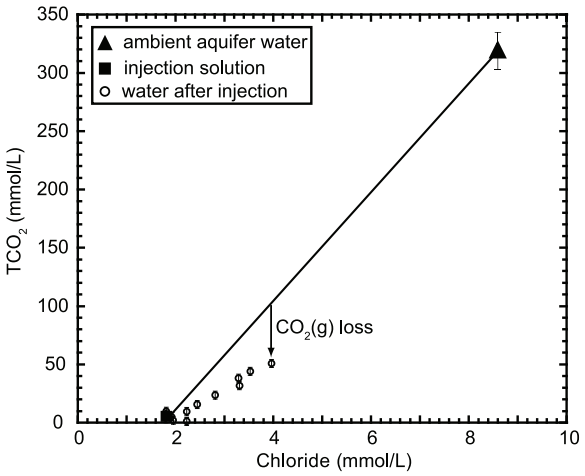

Figure 8. TCO_2 versus chloride, illustrating the mixing line between the injection solution and the ambient aquifer water as well as the data from water samples extracted after the injection. All the extracted water samples have smaller TCO_2 values as expected assuming linear mixing between the injected solution and the ambient groundwater, indicating CO_2(g) loss. Error bars are illustrated for TCO_2 values, whereas error bars for chloride are smaller than the markers.

dilution and mixing of the injected solution and trapping of the injected solution in lower transmissivity zones, such as pore-scale voids in the matrix rock [*Altman et al.*, 2002].

[27] In addition to the heterogeneity of the formation, the mass recovery rate and loss of the injected CO_2 are influenced by the drift of the solution with the natural groundwater flow during the incubation period. How far the solution drifts away during the incubation phase is a function of the porosity, permeability, the regional hydraulic gradient and the duration of the resting phase. Among all these factors, the regional hydraulic gradient has the strongest effect on the mass recovery rates, according to *Altman et al.* [2002]. Furthermore, regional advective flow velocity, and therefore the drift of an injected solution, can be estimated on the basis of a single-well tracing method [*Leap and Kaplan*, 1988]. The method requires accurate data of permeability, effective porosity and regional hydraulic gradient. Unfortunately, the hydraulic gradient is not well defined in the testing area due to a lack of multiple observation wells and we cannot quantitatively evaluate the effect of drift on the estimated mass recovery rate. We assume that the heterogeneity of the formation is strong due to fracture porosity in the capture/injection zone with large transmissivity contrasts above and below. Enhanced mixing and potential dilution of the injected solution during groundwater drift within the capture/injection zone resulted in reduced mass recovery (approximately 60% by volume), corresponding to a partial loss of the injected CO_2.

7. Implications for CO_2 Sequestration

[28] The release of cations such as Ca, Mg, and Na by acid neutralization sets the stage for the formation of secondary carbonate minerals and the mineral trapping of injected CO_2. For CO_2 sequestration, the mineral trapping potential of a target formation depends on the in situ release rates of alkaline earths, and to a minor extent, of alkali elements. Deep aquifers (>800 m) are preferred for CO_2 sequestration because pressure and temperature conditions tend to preserve the injected CO_2 in a supercritical state. The formation of carbonic acid and water-rock reactions depend on the solubility of supercritical CO_2 in water, which depends on pressure, temperature and salinity. *Enick and Klara* [1990], *Blencoe et al.* [2001], and *Duan and Sun* [2003] have all conducted laboratory studies of the solubility of CO_2 at conditions close to those for deep CO_2 sequestration targets. The relatively shallow (~230 m) and low temperature (13°C) target of this study, however, precludes P-T conditions sufficient for sustaining injection of supercritical CO_2. Nevertheless, in these relatively permeable Ca-Mg silicate rocks, we observe rapid acid neutralization rates and water-rock reactions sufficient for safe and permanent geologic storage of CO_2. The post-injection evolution of pH within the aquifer is also important because low pH facilitates the dissolution of Ca, Mg silicate minerals and high pH facilitates the precipitation of (Ca, Mg)CO_3. On the basis of our experimental results, and applying an average bulk rock dissolution rate of 0.138 mol/m^2/hour, a 1000 m^3 volume of CO_2 saturated water at P_{CO2} = 8 atm (3.2 x 10^8 mmol CO_2) would be neutralized (i.e., P_{CO2} back to initial 350 μatm) in approximately 19 hours after injection. Because dissolution rates of minerals increase with increasing temperature, we anticipate that both the acid neutralization and dissolution rates will proceed more rapidly in deeper (>800 m) and higher temperature (>80°C) aquifers. Concerning the storage capacity of basaltic rocks, conservative estimates of the CO_2 storage capacity in the Columbia River Basalt Group are over 100 billion tons of CO_2 [*McGrail et al.*, 2003]. However, the scale of porosity reduction

as a result of clay and calcium carbonate precipitation is unknown.

8. Conclusion

[29] We demonstrate an injection of carbonated water (P_{CO2} = 8 atm; pH = 3.5) in a single-well push-pull test and observe in situ cation release rates. Mixing between the injected solution and the ambient aquifer water as well as the subsequent water-rock reactions neutralize the carbonic acid and increase pH to ambient conditions (pH = 8.3) within hours. The injected acid induced a diversity of water-rock reactions including the release of alkaline earth metals and alkali metals from the formation. Calcium and magnesium release rates decrease as a function of pH and time because acidity decreases as a function of dilution and the proceeding water-rock reactions. Laboratory experiments on crushed bulk rock samples confirm the pH dependence of the release rate. An observed difference between the laboratory and field-based release rates could be partly attributed to the unconstrained estimate of the reactive surface area in the field experiment, which however remains speculative. In addition, differences in the mineralogy and experimental setup with dissolved CO_2 in field experiment versus HCl in laboratory experiment, as well as additional calcium (calcite) in the field experiment have also contributed to the 2.5 to 3.5 order magnitude difference between the dissolution rates. Mass balance models indicate that changes in the solution chemistry after injection can be explained by the dissolution of minerals such as plagioclase and pyroxene, which are the most abundant minerals in the injection zone, and by CO_2 loss. Overall, the mass recovery rate of 60% is most likely the result of injection solution and CO_2 loss in low-transmissivity matrix porosity within the contact zone and potential drift of the injected solution with groundwater flow beyond the injection/capture zone in this experiment.

[30] The results of this study emphasize the importance of defining cation release rates under in situ injection conditions for evaluation of a target formation for CO_2 sequestration. Low water-rock ratios, the presence of a multimineral environment, and in situ hydrological properties, all introduce significant effects on water-rock reactions after CO_2 injection. Single-well push pull tests enable experimental study of dilution through mixing, degassing and bulk rock dissolution rates, which therefore can provide information about the mineral trapping potential of a target aquifer. Similar studies in deep aquifers are needed to investigate these in situ reactions at higher formation temperature and pressure, higher P_{CO2}, and higher ionic strength conditions in similar Ca-Mg silicate formations. Quantifying the mineral trapping potential of such deep permeable reservoirs will underscore their efficacy for permanent and secure geological storage of industrial CO_2.

Acknowledgments

[31] This study was financially supported by the Lamont-Doherty Earth Observatory of Columbia University, the Columbia Earth Institute, the Comer Science and Education Foundation, and the Center de Recherches sur le Stockage Géologique du CO_2, Institut de Physique du Globe de Paris-Total-Schlumberger ADEME partnership. We thank Martin Stute (Lamont-Doherty Earth Observatory) for providing support for the anion analysis. Fieldwork and data acquisition were technically supported by W. Masterson and G. Myers (Lamont-Doherty Earth Observatory), and the laboratory experiments were conducted by Brian Maurizi and Zach Alessi-Friedlander as a part of the Lamont Summer Internship program supported by NSF. The manuscript benefited greatly from reviews by Karsten Pruess and one anonymous reviewer. LDEO contribution 697.

References

Altman, S. J., L. C. Meigs, T. L. Jones, and S. A. McKenna (2002), Controls of mass recovery rates in single-well injection-withdrawal tracer tests with a single-porosity, heterogeneous conceptualization, *Water Resour. Res.*, *38*(7), 1125, doi:10.1029/2000WR000182.

Assayag, N., J. M. Matter, M. Ader, D. Jézéquel, and P. Agrinier (2005), Carbon stable isotopes to monitor the reactivity of injected CO_2 in geological reservoirs, *Geophys. Res. Abstr.*, *7*, abstract 06930.

Bachu, S., W. D. Gunter, and E. H. Perkins (1994), Aquifer disposal of CO_2: Hydrodynamic and mineral trapping, *Energy Convers. Manage.*, *35*(4), 269–279.

Baines, S. J., and R. H. Worden (2004), The long-term fate of CO_2 in the subsurface: Natural analogues for CO_2 storage, in *Geological Storage of Carbon Dioxide*, edited by S. J. Baines and R. H. Worden, *Geol. Soc. Spec. Publ.*, *233*, 59–85.

Bergman, P. D., and E. M. Winter (1995), Disposal of carbon dioxide in aquifers in the U.S., *Energy Convers. Manage.*, *36*(6–9), 523–526.

Blencoe, J. G., et al. (2001), The CO_2–H_2O system: III. A new experimental method for determining liquid-vapor equilibria at high supercritical temperatures, *Am. Mineral.*, *86*(9), 1100–1111.

Burbery, L., G. Cassiani, G. Andreotti, T. Ricchiuto, and K. T. Semple (2004), Single-well reactive tracer test and stable isotope analysis for determination of microbial activity in a fast hydrocarbon-contaminated aquifer, *Environ. Pollut.*, *219*, 321–330.

Carroll, S. A., and K. G. Knauss (2005), Dependence of labradorite dissolution kinetics on CO_2(aq), Al (aq), and temperature, *Chem. Geol.*, *217*(3–4), 213–225.

Chipman, D. W., J. Marra, and T. Takahashi (1993), Primary production at 47°N and 20°W in the North Atlantic Ocean: A comparison between the ^{14}C incubation method and the mixed layer carbon budget, *Deep Sea Res., Part II*, *40*(1/2), 151–169.

Duan, Z., and R. Sun (2003), An improved model calculating CO_2 solubility in pure water and aqueous NaCl solutions form 273 to 533 K and from 0 to 2000 bar, *Chem. Geol.*, *193*, 257–271.

Enick, R. M., and S. M. Klara (1990), CO_2 solubility in water and brine under reservoir conditions, *Chem. Eng. Commun.*, *90*, 23–33.

Ganor, J., E. Roueff, Y. Erel, and J. D. Blum (2005), The dissolution kinetics of a granite and its minerals: Implications for comparison between laboratory and field dissolution rates, *Geochim. Cosmochim. Acta*, *69*(3), 607–621.

Giammar, D. E., R. G. Bruant, Jr., and C. A. Peters (2005), Forsterite dissolution and mangesite precipitation at conditions relevant for deep saline aquifer storage and sequestration of carbon dioxide, *Chem. Geol.*, *217*(3–4), 257–276.

Gislason, S. R., and H. P. Eugster (1987), Meteoric water-basalt interactions. I. A laboratory study, *Geochim. Cosmochim. Acta*, *51*, 2827–2840.

Goldberg, D., and K. Burgdorff (2005), Natural fracturing and petrophysical properties of the Palisades dolerite sill, in *Petrophysical Properties of Crystalline Rocks*, edited by P. K. Harvey et al., *Geol. Soc. Spec. Publ.*, *240*, 25–36.

Gunter, W. D., and E. H. Perkins (1993), Aquifer disposal of CO_2–rich gases: Reaction design for added capacity, *Energy Convers. Manage.*, *34*, 9–11.

Gunter, W. D., B. Wiwchar, and E. H. Perkins (1997), Aquifer disposal of CO_2–rich greenhouse gases: Extension of the time scale of experiment for CO_2–sequestering reactions by geochemical modeling, *Mineral. Petrol.*, *59*(1–2), 121–140.

Gunter, W. D., S. Bachu, and S. Benson (2004), The role of hydrogeological and geochemical trapping in sedimentary basins for secure geological storage of carbon dioxide, in *Geological Storage of Carbon Dioxide*, edited by S. J. Baines and R. H. Worden, *Geol. Soc. Spec. Publ.*, *233*, 129–145.

Hänchen, M., V. Prigiobbe, G. Storti, T. M. Seward, and M. Mazzotti (2006), Dissolution kinetics of fosteritic olivine at 90–150°C including effects of the presence of CO_2, *Geochim. Cosmochim. Acta*, *70*, 4403–4416.

Hawkins, D. G. (2004), No exit: Thinking about leakage from geologic carbon storage sites, *Energy*, *29*, 1571–1578.

Hitchon, B. (1996), *Aquifer Disposal of Carbon Dioxide: Hydrodynamic and Mineral Trapping—Proof of Concept*, Geoscience, Alberta, Canada.

Hoffert, M. I., et al. (2002), Advanced technology paths to global climate stability: Energy for a greenhouse planet, *Science*, *298*, 981–987.

Holland, H. D., B. Lazar, and M. McCaffrey (1986), Evolution of the atmosphere and the oceans, *Nature*, *320*, 27–33.

Holloway, S. (2001), Storage of fossil fuel-derived carbon dioxide beneath the surface of the Earth, *Annu. Rev. Energy Environ.*, *26*, 145–166.

Intergovernmental Panel on Climate Change (IPCC) (2005). *IPCC Special Report on Carbon Dioxide Capture and Storage: Prepared by Working Group III of the Intergovernmental Panel on Climate Change*, edited by P. Metz et al., 442 pp., Cambridge Univ. Press, New York.

Istok, J. D., M. D. Humphrey, M. H. Schroth, M. R. Hyman, and K. T. O'Reilly (1997), Single-well, "push-pull" tests for in situ determination of microbial activities, *Ground Water*, *35*(4), 619–631.

Istok, J. D., J. A. Field, M. H. Schroth, B. M. Davis, and V. Dwarakanath (2002), Single-well "push-pull" partitioning tracer test for NAPL detection in the subsurface, *Environ. Sci. Technol.*, *36*, 2708–2716.

Johnson, J., G. Anderson, and D. Parkhurst (2000), Database 'thermo.com.V8.R6.230,' *Rev. 1.11*, Lawrence Livermore Natl. Lab., Livermore, Calif.

Kaszuba, J. P., D. R. Janecky, and M. G. Snow (2005), Experimental evaluation of mixed fluid reactions between supercritical carbon dioxide and NaCl brine: Relevance to the integrity of a geologic carbon repository, *Chem. Geol.*, *217*(3–4), 277–293.

Lackner, K. S. (2003), A guide to CO_2 sequestration, *Science*, *300*, 1677–1678.

Leap, D. I., and P. G. Kaplan (1988), A single-well tracing method for estimating regional advective velocity in a confined aquifer: Theory and preliminary laboratory verification, *Water Resour. Res.*, *24*(7), 993–998.

Matter, J. M., D. S. Goldberg, R. H. Morin, and M. Stute (2005), Contact zone permeability at intrusion boundaries: New results from hydraulic testing and geophysical logging in the Newark Rift Basin, *Hydrogeol. J.*, *14*, 689–699.

McGrail, B. P., A. M. Ho, S. P. Reidel, and H. T. Schaef (2003), Use and features of basalt formations for geologic sequestration, in *Proceedings of the Sixth International Conference on Greenhouse Gas Control Technologies*, vol. II, edited by J. Gale and Y. Kaya, pp. 1637–1640, Elsevier, New York.

McLing, T. L., R. W. Smith, and T. M. Johnson (2001), Chemical characteristics of thermal water beneath the eastern Snake River Plain, *Spec. Pap. Geol. Soc. Am.*, *353*, 205–211.

Pacala, S., and R. Socolow (2004), Stabilization wedges: Solving the climate problem for the next 50 years with current technologies, *Science*, *305*, 968–971.

Parkhurst, D. L., and C. A. J. Appelo (1999), User's guide to PHREEQC (version 2)—A computer program for speciation, batch-reaction, one-dimensional transport, and inverse geochemical calculations, *U.S. Geol. Surv. Water Resour. Invest.*, *Rep. 99-4259*.

Pearce, J. M., S. Holloway, H. Wacker, M. K. Nelis, C. Rochelle, and K. Bateman (1996), Natural occurrences as analogues for the geological disposal of carbon dioxide, *Energy Convers. Manage.*, *37*(6–8), 1123–1128.

Pokrovsky, O. S., and J. Schott (2000), Kinetics and mechanism of forsterite dissolution at 25°C and pH from 1 to 12, *Geochim. Cosmochim. Acta*, *64*(19), 3313–3325.

Rimstidt, C. D. (1997), Quartz solubility at low temperatures, *Geochim. Cosmochim. Acta*, *61*(13), 2553–2558.

Rochelle, C. A., I. Czernichowski-Lauriol, and A. E. Milodowski (2004), The impact of chemical reactions on CO_2 storage in geological formations: A brief review, in *Geological Storage of Carbon Dioxide*, edited by S. J. Baines and R. H. Worden, *Geol. Soc. Spec. Publ.*, *233*, 87–106.

Sass, B., J. Gupta, J. Ickes, M. Eagelhard, P. D. Bergman, and C. Byaer (2001), Interaction of rock minerals with CO_2 and brine: A hydrothermal investigation, paper presented at First National Conference on Carbon Sequestration, Off. of Sci. and Off. of Fossil Energy, U.S. Dep. of Energy, Washington, D. C., 15–17 May.

Spane, F. A., and W. D. Webber (1995), Hydrochemistry and hydrogeologic conditions within the Hanford Site upper basalt confined aquifer system, *PNL-10817*, Pac. Northw. Natl. Lab., Richland, Wash.

Takahashi, T., D. Goldberg, and J. C. Mutter (2000), Secure, long-term sequestration of CO_2 in deep saline aquifers associated with oceanic and continental basaltic rocks, in *Proceedings of the SRI International Symposium "Deep Sea & CO2 2000,"* Ship Res. Inst., Mitaka, Japan. (Available at http://www.srimot.go.jp/co2/index.html)

Velbel, M. A. (1993), Constancy of silicate-mineral weathering-rate ratios between natural and experimental weathering: Implications for hydrologic control of differences in absolute rates, in *Geochemical Kinetics of Mineral-Water Reactions in the Field and the Laboratory*, edited by S. L. Brantley and M. A. Velbel, *Chem. Geol.*, *105*, 89–99.

White, A. F., and S. L. Brantley (2003), The effect of time on weathering of silicate minerals: Why do weathering rates differ in the laboratory and field?, *Chem. Geol.*, *202*, 479–506.